Invited paper

OPTO-ELECTRONICS REVIEW **10**(3), 159–174 (2002)

HgCdTe infrared detectors♣

P. NORTON*

Santa Barbara Research Center, Raytheon Systems Company, 75 Coromar Drive, Goleta, CA 93117, USA

HgCdTe infrared detectors have been intensively developed over the past forty years since the first synthesis of this compound semiconductor in 1958. Today, HgCdTe is the most widely used infrared detector material. This paper reviews key developments in the crystal growth and device history of this important technology. Projections and challenges for the continued evolution of this technology are summarized.

Keywords: HgCdTe single crystals and epitaxial layers, HgCdTe photoconductors and photodiodes, focal plane arrays.

1. Introduction

HgCdTe was first synthesized in 1958 by a research group led by Lawson [1] at the Royal Radar Establishment in England. This work was the successful outcome of a deliberate effort to engineer a direct-bandgap, intrinsic semiconductor for the long wavelength infrared (LWIR) spectral region (8–14 μm). Early recognition of the significance of this work led to intensive development in a number of countries including England, France, Germany, Poland, the former Soviet Union and the United States [2]. Little has been written about the early development years – the existence of work going on in the United States was classified until the late 60 s. The French pavilion at the 1967 Montreal Expo illustrated a CO_2 laser system with a photovoltaic HgCdTe detector. Photoconductive devices had been built in the US as early as 1964 at Texas Instruments.

Advancement of the crystal growth technology has proceeded deliberately and steadily for four decades in spite of the high vapour pressure of Hg at the melting point of HgCdTe and the known toxicity of the material. The first section of this paper reviews a key properties of HgCdTe which are crucial for IR detector functions. Progress made in growing HgCdTe is then summarized and the capabilities of bulk, liquid-phase, and vapour-phase epitaxy are then compared.

HgCdTe has inspired the development of three "generations" of detector devices which are described in the subsequent three sections. The first generation, linear arrays of photoconductive detectors, has been produced in large quantities and is in widespread use today. The second generation, two-dimensional arrays of photovoltaic detectors, is now in high-rate production – thousands of arrays annually. Third generation devices, defined here to encompass the more exotic device structures embodied in two-colour detectors, avalanche photodiodes, and hyperspectral arrays, are now fielded in demonstration programs. These devices offer functionality beyond today's detectors, but are some years away from high-rate production.

Even as third-generation detector development proceeds, device performance is being enhanced in a number of directions: array size, cooling requirements, long wavelength application of photovoltaic technology, three-colour, and readout capability. The direction of this work is summarized in the final section.

2. HgCdTe material

Several properties of HgCdTe qualify it as highly useful for infrared detection. These are:

- Adjustable bandgap from 0.7 to 25 μm.
- Direct bandgap with high absorption coefficient.
- Moderate dielectric constant/index of refraction.
- Moderate thermal coefficient of expansion.
- Availability of wide bandgap lattice-matched substrates for epitaxial growth.

We now discuss each of these key properties.

Infrared detection in HgCdTe begins with the excitation of an electron from the valence band into the conduction band. The minimum photon energy required is equal to the bandgap, E_g. The bandgap of $Hg_{1-x}Cd_xTe$ is a function of the alloy composition ratio "x" of CdTe to HgTe, and the temperature of the material. A number of equations have been developed to summarize the empirically measured relationship. One of these, developed by Hansen *et al.* [3] is given by the expression:

$$E_g = -0.302 + 1.93x - 0.81x^2 + 0.832x^3 + \\ + 5.35(1-2x)10^{-4}T. \quad (1)$$

*e-mail: p.norton@verizon.net

♣ The paper presented there appeared in *Proc. Sixth Inter. Symp. Long Wavelength Infrared Detector and Arrays,* Electrochem Soc. Proc. 98-21, pp. 48–70, New Jersey, 1999. (Reprinted with permission of ECS)

Figure 1 illustrates the dependence of this equation for representative compositions of the alloy, x = 0.2, 0.3, and 0.4, which span the medium-to-long wavelength spectral regions, 3–14 μm. With higher values of x the spectral response can be tailored to wavelengths as short as 0.7 μm, corresponding to the bandgap of CdTe. Since the bandgap of HgTe is negative, or inverted, the alloy can be grown to achieve arbitrarily small bandgaps. In practice, HgCdTe has not been used significantly beyond about 25 μm.

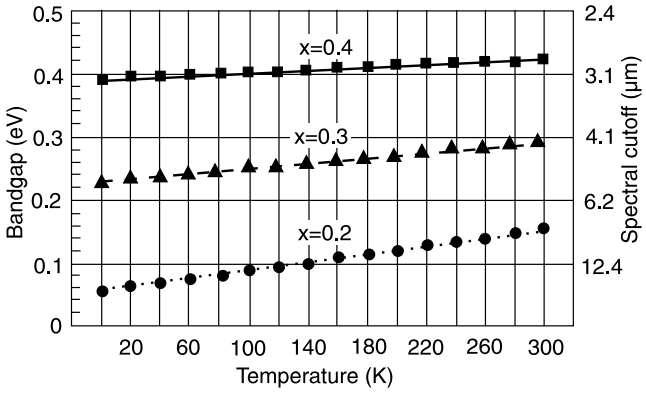

Fig. 1. Bandgap and corresponding spectral cutoff for representative alloy compositions of $Hg_{1-x}Cd_xTe$ as a function of temperature as calculated from Eq. (1).

Direct bandgap semiconductors, such as HgCdTe, have a sharp onset of optical absorption as the photon energy increases above E_g. In contrast, indirect semiconductors, such as silicon or germanium, have softer absorption curves. The optical absorption coefficient for HgCdTe has been measured by Scott [4] and is illustrated in Fig. 2 for a wide range of alloy compositions.

Strong optical absorption allows HgCdTe detector structures to absorb a very high percentage of the signal while being relatively thin, on the order of 10–20 μm. Minimizing the detector thickness helps to minimize the volume

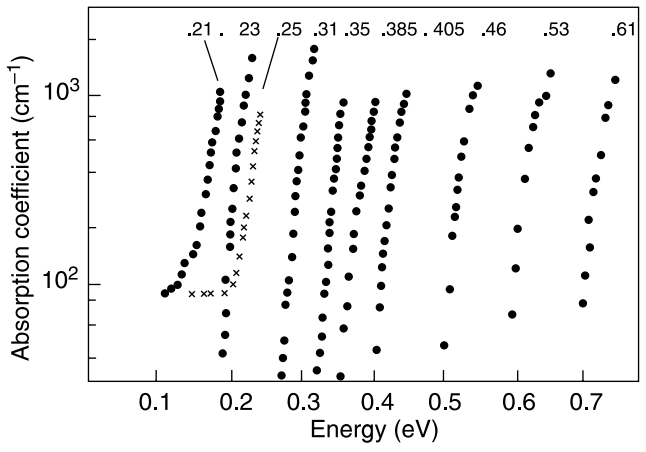

Fig. 2. Optical absorption coefficient of $Hg_{1-x}Cd_xTe$ as a function of composition x (after Ref. 4).

of material which can generate noise, thermal excess carriers, in the diffusion-limited operating mode.

The difficulties in growing HgCdTe material, significantly due to the high vapour pressure of Hg, encouraged the development of alternative detector technologies over the past forty years. One of these was PbSnTe, a IV–VI compound material system that was vigorously pursued in parallel with HgCdTe in the late 60s and early 70s. PbSnTe was comparatively easy to grow and good quality diodes on alloy compositions tailored for the 8–12 μm spectral region were readily demonstrated. Two factors led to the abandonment of PbSnTe detector work in the United States by the mid-70s:

- High dielectric constant of PbSnTe compared with HgCdTe.
- Large temperature coefficient of expansion (TCE) mismatch with Si.

The static dielectric constant, ε_0, is about 400 in PbTe [5] and 1770 in SnTe [6]. The resulting high capacitance of PbSnTe diodes gave long RC time constants. Scanned infrared imaging systems of the 70s required relatively fast response times so that the scanned image is not smeared in the scan direction. With the trend today towards staring arrays for many applications, this consideration might be less important than it was when first generation systems were being designed.

The second reason that high capacitance photovoltaic detectors are undesirable is because diode capacitance drives the noise in the silicon readout circuits which amplify the photosignals. This is particularly undesirable for low-background flux applications where the photon noise levels are low.

The second drawback to PbSnTe was its large TCE. Today's hybrid detector structures are built with an indium-bump bonded interface between silicon readout and the detector array. Differences in the TCE between the readout and detector substrate can lead to failure of the indium bonds after repeated thermal cycling from room temperature to the cryogenic temperature of operation. The TCE CdTe [7] is about 6×10^{-6}, while that of PbSnTe [8] is in the range of 20×10^{-6}. This results in much greater TCE mismatch with silicon (TCE about 3×10^{-6} [9]) readouts for hybrid structure assemblies. It might be noted that both Ge and GaAs have TCE values close to HgCdTe, giving detectors based on those materials no significant advantage in this respect.

How restrictive is the TCE mismatch for hybrid structures? Large hybrid structures of HgCdTe combined with silicon readouts, having linear dimensions greater than 1 cm, have been built and tested with thermal-cycle reliability in excess of several thousand cycles. The eventual progression to larger array sizes will likely lead to increasing emphasis on growth technologies capable of growing HgCdTe layers directly on silicon substrates.

The final key property we address is the availability of lattice-matched substrates for epitaxial growth. Epitaxial growth is now used almost exclusively for HgCdTe detec-

tor array production. About 15 years ago it was found that the crystal perfection and surface morphology of the epitaxial layers was significantly influenced by the substrate-epitaxial layer lattice constant mismatch. This was discovered when about 4% ZnTe was added to CdTe to tune the substrate lattice constant to match HgCdTe. A great advantage of this II-VI alloy system is the narrow range of lattice constant variation from CdTe to HgTe, as illustrated in Fig. 3.

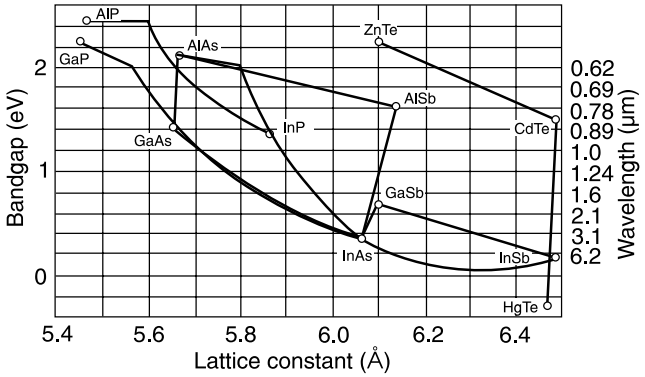

Fig. 3. Comparison of the bandgap vs. lattice constant variation with alloy composition for $Hg_{1-x}Cd_xTe$ and CdZnTe substrates, with the lattice constant for a variety of III-V compounds (after Ref. 10). $Cd_{0.96}Zn_{0.04}Te$ is a good match for a wide range of MWIR to LWIR HgCdTe alloys.

By comparison, the availability of lattice-matched substrates for III-V alloys is limited in many cases. InP is suitable for InGaAs alloys with a bandgap near 0.75 eV (1.65 μm) in the short wavelength infrared (SWIR) region. However, as the alloy is varied to longer wavelengths, the crystal and device quality of InGaAs degrades so that it is restricted to wavelengths of about 2.4 μm or shorter. The close lattice matching of GaAs to AlAs supports the growth of quantum well structures with good crystal quality. However, the extrinsic-like properties of quantum well devices require cooling to lower temperatures than intrinsic semiconductors such as HgCdTe, for equivalent spectral wavelength cutoff response [11–16].

An extensive review of the properties of HgCdTe and related alloys has been recently published by Capper [17].

3. Growth of HgCdTe

The growth of HgCdTe has evolved along with other semiconductor materials technologies over the past 40 years. Three principal methods have been developed:

- Bulk.
- Liquid phase epitaxy – LPE.
- Vapour phase epitaxy – VPE.
  - Metalorganic chemical vapour deposition – MOCVD.
  - Molecular beam epitaxy – MBE.

The time line for the evolution of growth technologies is illustrated in Fig. 4.

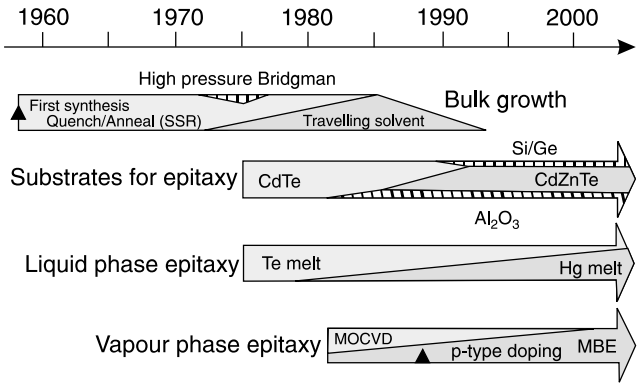

Fig. 4. Evolution of HgCdTe crystal growth technology from 1958 to present. Thin epitaxial layers allow nearly 100% absorption. Epitaxial methods replaced bulk growth by the early 90s. High quality substrates for epitaxy had to be developed before this transition took place. LPE is the dominant production method used today. MBE is used to grow advanced device structures which are difficult to realize with LPE.

3.1. Bulk crystal growth

Bulk growth of HgCdTe proved very difficult due mainly to the high vapour pressure of Hg at the crystal melting point, about 950°C. Early experiments and a significant fraction of early production was done using a quench-anneal or solid-state recrystallization process. In this method the alloy was reacted from purified starting materials and then rapidly quenched. Rapid quenching was needed to prevent segregation of HgTe from CdTe which have significantly different melting temperatures. The result of quenching was a highly polycrystalline solid. Annealing near the melting point was used to grow larger grains.

Bridgman growth, under high pressure to contain the Hg pressure, was attempted for several years near the mid-70s. At the same time, solvent growth methods were initiated which could be carried out at reduced temperature. In one case the solvent used was Te. Solvent growth also provided an additional purification step through zone refining as the solution was passed through the solid phase. By the late 70s bulk growth was sufficiently reproducible to support the production start-up of first generation LWIR photoconductive HgCdTe array production.

Bulk growth produced thin rods of HgCdTe material, generally 8-to-12 mm in diameter and about 20 cm in length. This material could be used for linear array production, but the vision of larger two-dimensional arrays could not be realized with this method. Another drawback to bulk material was the need to thin the bulk wafers, generally cut about 500 μm thick, down to the final device thickness of about 10 μm. Polishing the wafers, mounting them to suitable substrates, and polishing to the final device thickness was labor intensive.

In the early 90s, bulk growth of HgCdTe was phased out for the routine production of first generation photo-

conductive devices. Bulk growth has been replaced by liquid phase epitaxial (LPE) growth which is reviewed following a description of substrates for epitaxial growth below.

3.2. Substrates for epitaxial growth

Epitaxial growth of thin layers of HgCdTe for infrared detector array fabrication requires a suitable substrate. CdTe was used initially, since it was available from commercial sources in reasonably large sizes. Unlike HgCdTe, CdTe bulk crystal growth is not limited by high Hg overpressures. The <111> crystal orientation was determined to be favourable for smooth growth by the LPE technique. For vapour phase growth, the <211> orientation gave preferential growth with the MBE technique.

CdTe has good physical properties for an infrared detector substrate. First of all it is transparent out to 30 μm, so that devices with the IR photon-flux incident on the backside are readily made without having to remove the substrate. Second, CdTe is not a potential dopant of the epitaxial film. Third, CdTe is more robust than HgCdTe crystals, although still much more fragile than silicon or germanium. The main drawback to CdTe as an epitaxial substrate is that it has a few percent lattice mismatch with LWIR and middle wavelength infrared (MWIR) HgCdTe. This mismatch caused LPE-grown films to be morphologically rougher than desired.

By the mid-80s it was demonstrated that the addition of a few percent ZnTe to CdTe could create a lattice-matched substrate. CdZnTe has been the principal substrate in use since that time. It is available from a variety of vendors today. Figure 5 illustrates a furnace and controller used to grow CdZnTe crystals with the modified Bridgman technique. Figure 6 shows two large boules grown by the technique. Following boule growth the CdZnTe material is polycrystalline, but with very large grains. An effective method for seeding the growth to produce oriented single-crystal boules had not been developed. The largest grain is selected and oriented for sawing into wafers. After sawing, the wafers are polished in preparation for epitaxial growth. Defect densities of CdZnTe substrates are routinely in the low 10^4 cm^{-2} range as determined by etch pit counts. Two such wafers are shown in Figure 7.

Fig. 5. Furnace and controller for growing CdZnTe boules.

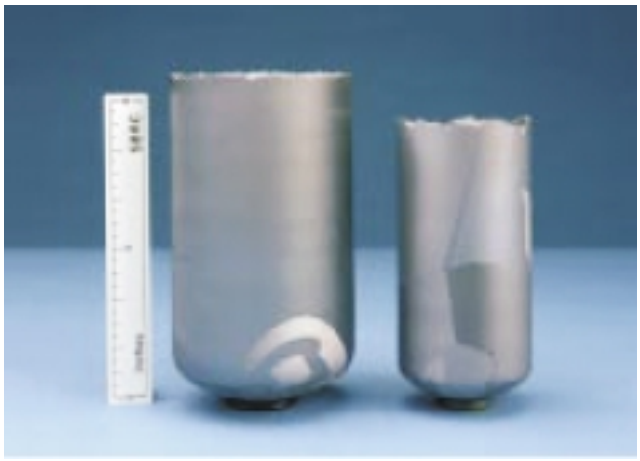

Fig. 6. CdZnTe boules grown by the modified Bridgman method. These boules are 2.6 and 3.6 inches in diameter (6.7 and 9.2 cm). The large grain structure of the crystals is visible. The boules are sawn into wafers for epitaxial growth of HgCdTe films.

Sapphire has also been widely used as a substrate for HgCdTe epitaxy. In this case a CdTe film is deposited on the sapphire prior to the growth of HgCdTe. Sapphire has excellent physical properties and can be purchased in large wafer sizes. It has a fairly large lattice constant mismatch with HgCdTe which the CdTe buffer layer overcomes to a great extent. The thermal coefficient of expansion of sapphire is a better match to silicon than CdZnTe. Defect densities of sapphire substrates prepared for epitaxial growth of HgCdTe are typically in the mid-10^5 cm^{-2} range. Sap-

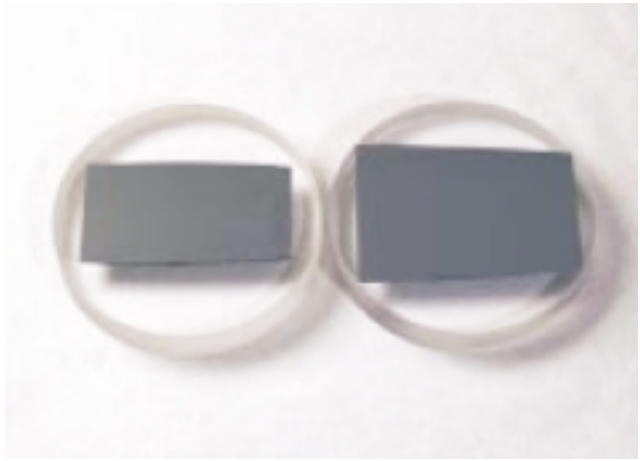

Fig. 7. CdZnTe wafers after sawing and polishing. The wafers are mounted on optical flats.

phire is transparent from the UV to about 6 μm and has been used for the production of a significant number of SWIR and MWIR HgCdTe photovoltaic arrays. It is not applicable to backside-illuminated LWIR arrays because of the opacity of sapphire beyond 6 μm.

Germanium has been used experimentally, together with CdTe buffer layers, to grow HgCdTe epitaxial films. Germanium has good physical properties and is transparent from 2 μm out to about 20 μm, falling off gradually at longer wavelengths. CdTe buffer layers enable epitaxial growth of reasonable quality HgCdTe. Germanium's TCE is very close to that of HgCdTe, and consequently also has a significant mismatch to silicon readouts. Germanium offers no particular advantage and only a few examples of its use are known.

Silicon substrates are the "holy grail" of substrate development. Silicon is strong, large, and has no thermal coefficient of expansion mismatch with silicon readouts. The rewards for the quest are matched by the substantial difficulties of growing II-VI materials on silicon. Work on silicon substrates began in the mid-80s and although progress has been slow it is still very promising. Buffer layers are needed to prime the surface prior to epitaxial growth. Defect densities of silicon substrates prepared for epitaxial growth of HgCdTe are typically in the 10^6 cm^{-2} range – improved by an order of magnitude from a decade ago. Still this technology needs additional development for use in applications which require high pixel operability, particularly for LWIR alloy compositions.

3.3. Liquid phase epitaxial growth

Liquid phase epitaxial (LPE) growth of thin layers on CdTe substrates began in the early-to-mid 70s. CdTe substrates could be grown in large diameters because Hg overpressure was not a limiting consideration. Initially, Te solutions with dissolved Cd and saturated with Hg vapour were used to efficiently grow HgCdTe layers with thickness suitable for direct device fabrication. Cd has a high solubility in Te. This allowed small-volume melts to be used with the slider technique which did not appreciably deplete during the growth run. Surface wetting and melt decanting were early problems however.

Experiments with Hg-solvent LPE began in the late 70s, a couple years after the initial work with Te solutions. Because of the limited solubility of Cd in Hg, the volume of the Hg melts had to be much larger than Te melts in order to minimize melt depletion during layer growth. This precluded the slider growth approach. Hg-melt epitaxy has been developed using large dipping vessels. Two Hg-melt LPE growth systems are pictured in Fig. 8. Each system in this photo is capable of growing on a total of 60 cm^2 of substrate area per growth run.

LPE growth struggled in the early 80s as growers learned a series of important lessons in order to reduce surface morphology defects and achieve uniform, smooth epitaxial layers. One of these was the importance of having precise substrate orientation. A second was the need for lattice-matched substrates which were developed by adding a few percent of ZnTe to CdTe.

Fig. 8. Vertical dipping Hg-melt LPE growth systems employ vessels containing several kg of Hg saturated with Cd. In addition to the Cd, dopants are added to produce either n- or p-type HgCdTe epitaxial films.

Diodes fabricated on early LPE material were made by ion implantation into p-type layers which had been annealed to generate Hg-vacancy acceptors. By the mid-80s, LPE growers learned how to achieve extrinsic p-and n-type doping, allowing the growth of junctions using p- and n-type doped melts. This resulted in greatly improved device quality and set the stage for the production of both first- and second-generation devices from LPE material.

LPE growth technology is now very mature for production of both first- and second-generation tactical detectors. Hundreds or thousands of layers are routinely grown each year for a wide variety of production programs as well as technology demonstration and technology development tasks. Even so, LPE technology is limited for a variety of advanced HgCdTe structures to be described later in this paper. These devices require more elaborate layer structures than a p^+-n junction. The gradient in x-value, a consequence of the partial depletion of Cd during the operation, can generate a barrier to carrier transport in certain cases. LPE also typically melts off a thin layer of the underlying material each time an additional layer is grown. These limitations have provided an opportunity for vapour-phase growth to supplant LPE technology for growing advanced device structures in the near term. An overview of vapour phase growth is described in the next section.

3.4. Vapour phase epitaxial growth

Like the Viking expeditions to North America, early vapour phase researchers left behind very few artifacts. Vacuum evaporation growth of HgCdTe was explored as

early as the late 60s at an IBM facility. Bulk HgCdTe was also assembled into sputtering targets and sputtered films were evaluated in a number of laboratories. Nothing came of these early efforts. Temperature-gradient-induced vapour transport has also been used to grow films in a few laboratories over the years as well.

The modern vapour phase era began in the early 80s with parallel efforts using metalorganic chemical vapour deposition (MOCVD) and molecular beam epitaxy (MBE). By this time both of these methods had been well established in the III-V semiconductor materials arena and were adapted for growing II-VI compounds and alloys.

Over the past fifteen years there have been a variety of groups who have explored MOCVD and MBE techniques. On the MOCVD front a wide variety of metalorganic compounds were developed along with a number of reaction-chamber designs. MBE technology, in parallel, had to address specially designed Hg-source ovens to overcome the low sticking coefficient of Hg at the growth temperature. A few attempts were made using hybrid systems, MOMBE for example, where metalorganic sources were used in an MBE chamber.

At this time, MBE has become the dominant vapour phase growth method for HgCdTe. Although the quality of MBE material is not yet on a par with LPE, it has made tremendous progress in the past decade to the point where a variety of high-background device formats have been successfully demonstrated using this growth technique. Keys to this success have been the ability to dope layers both p- and n-type, and the reduction of etch pit densities by an order of magnitude or more from a range of 10^7 cm^{-2} to below 10^6 cm^{-2}. An MBE system used to grow HgCdTe is shown in Fig. 9. MBE is now the preferred method for growing complex layer structures for two- and three-colour detectors as well as for avalanche photodiodes (APDs). It is anticipated that MBE will phase into production for a subset of applications in the next few years.

Fig. 9. HgCdTe MBE system. This system has a 5-inch (125 mm) susceptor to hold large substrates.

3.5. Comparison of growth techniques

The properties of HgCdTe grown by the variety of techniques discussed above are summarized in Table 1. The continuing evolution of HgCdTe materials and crystal growth technology is reviewed at a number of conferences each year as well as at other conferences held less frequently. A convenient reference is the proceedings of the U.S. Workshop on Physics and Chemistry of II-VI materials, published by the Journal of Electronic Materials [18].

4. HgCdTe infrared detector devices

4.1. Overview

The popularity of HgCdTe detectors is made possible by their flexibility in spectral response over a wide span of the infrared regions of interest. HgCdTe spectral flexibility is illustrated in Fig. 10 which shows the spectral quantum efficiency of a variety of HgCdTe devices, including photoconductors (PC), photodiodes (PV), and avalanche photodiodes (APDs). Photodiode technology is being vigorously extended to wavelengths beyond 12 μm. In the next few years, photodiodes will largely replace photoconductors at wavelengths out to about 20 μm. Single element photoconductors used in spectrometers to about 25 μm at liquid nitrogen temperature will continue to occupy that niche application.

Three generations of HgCdTe devices have been successively developed. The time evolution of this development is illustrated in Figure 11. Photoconductors, the first generation of HgCdTe devices, entered production in the late 70s following the establishment of reproducible bulk growth techniques and anodic-oxide surface passivation. In parallel work had begun on photovoltaic device technology

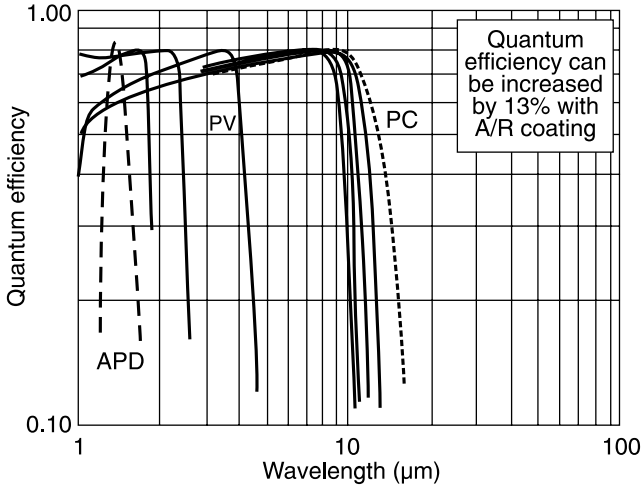

Fig. 10. Spectral quantum efficiency for HgCdTe devices without antireflection coating. Photodiodes span all but the longest wavelengths where photoconductors are still commonly used. At short wavelengths, avalanche photodiodes are in development. Antireflection coating raises the quantum efficiency to > 90%.

Table 1. Comparison of the various methods used to grow HgCdTe.

	Bulk			Liquid phase epitaxy		Vapour phase epitaxy	
	SSR	Travelling heater method					
		HCT melt	Te melt	Hg melt	Te melt	MOCVD	MBE
Temperature (°C)	950	950	500	350–550	400–550	275–400	160–200
Pressure (Torr)	150 000	150 000	760–8000	760–11400	760–8000	300–760	10^{-3}–10^{-4}
Growth rate (μm/hr)	250	250	80	30–60	5–60	2–10	1–5
Dimensions *w* (cm)	0.8–1.2 dia	0.8–1.2 dia	2.5 dia	5	5	7.5 dia	7.5 dia
l (cm)	–	–	–	6	5	4	4
t (cm)	15	15	15	0.0002–0.0030	0.0005–0.012	0.0005–0.001	0.0005–0.001
Dislocations (cm^{-2})	$<10^5$	–	$<10^5$	$<10^5$	$<10^5$–10^7	5×10^5–10^7	5×10^4–10^6
Purity (cm^{-3})	$<5\times10^{14}$	$<5\times10^{14}$	$<5\times10^{14}$	$<5\times10^{14}$	$<5\times10^{14}$	$<1\times10^{15}$	$<1\times10^{15}$
n-Type doping (cm^{-3})	N/A	N/A	N/A	1×10^{14}–1×10^{18}	1×10^{14}–1×10^{16}	5×10^{14}–5×10^{18}	5×10^{14}–1×10^{19}
p-Type doping (cm^{-3})	N/A	N/A	N/A	1×10^{15}–1×10^{18}	1×10^{15}–5×10^{16}	3×10^{15}–5×10^{17}	1×10^{16}–5×10^{18}
X-ray rocking curve (arc sec)	–	–	20–60	<20	<20	50–90	20–30
Compositional uniformity (Δx)	<0.002	<0.004	<0.005	<0.002	<0.002	±0.01–0.0005	±0.01–0.0006

which took another decade to reach volume production. At this time, third-generation devices are in development and demonstration programs. Each of these will be described below.

4.2. Photoconductors

First generation HgCdTe detectors consist of linear arrays of photoconductive devices. Good quality photoconductors can be fabricated by applying metal electrodes to pure n-type material, thinned to approximately 10 μm. The basic photoconductor device structure is illustrated in Fig. 12.

Characteristics of a basic LWIR photoconductive HgCdTe are:

- 50–100 Ω impedance per square.
- 10^5 V/W at 1 mA bias for a 50×50 μm device.
- D^* about 80% of background limit.
- Photon noise level of a few nV/Hz.

These detectors are tractable with low-noise preamplifiers, generally having emitter-coupled bipolar front ends.

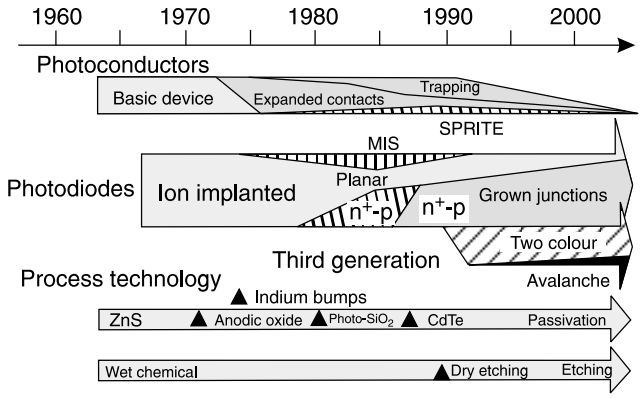

Fig. 11. A time line of the evolution of three generations of HgCdTe infrared detector devices and key developments in process technology which made them possible.

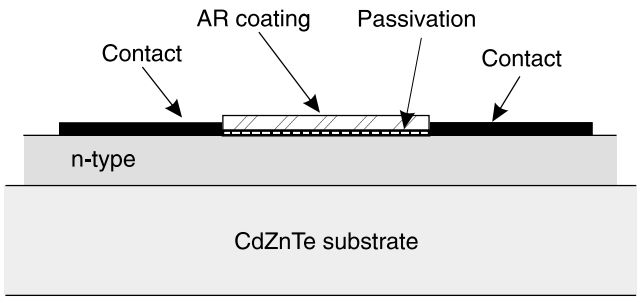

Fig. 12. Cross section of a basic HgCdTe photoconductor. The n-type layer of HgCdTe is approximately 10 μm thick. Typical photoconductors are passivated with anodic oxide and antireflection coated with zinc sulfide.

However, because of their low impedance and low noise, photoconductors have not been deployed with focal plane readouts operating at 80K – standard silicon bipolar devices do not operate below about 150 K. These factors have limited the scope of first generation devices to linear arrays with typically fewer than 200 elements. Within this scope the industry has produced tens of thousands of thermal imaging systems using PC arrays.

Two such systems have accounted for most of the production. The first of these is the Army Common Module. Imaging systems built with this approach were based on a family of arrays having 60, 120, or 180 elements, all with approximately 50 μm pixels. Figure 13 illustrates such an array.

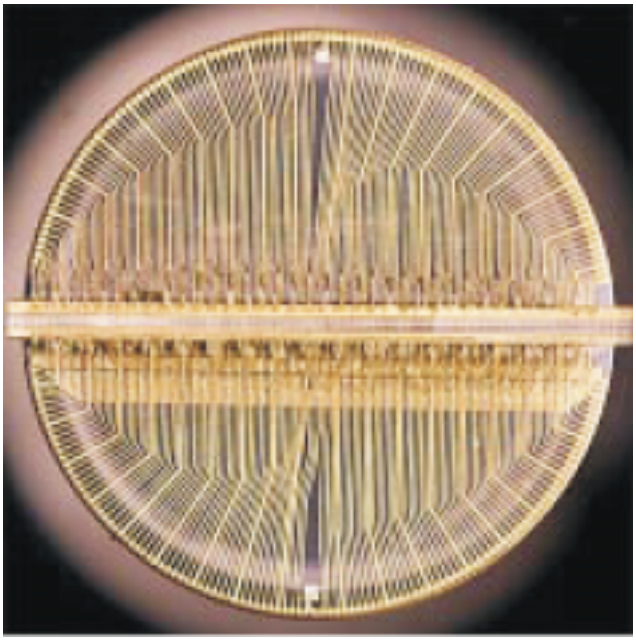

Fig. 13. 180 element Common Module linear array of HgCdTe photoconductive detectors. The array is mounted on the end of a glass cold finger and wire bonded to metallized leads which interface to warm preamplifiers and bias circuits through a vacuum interface. Over 200 wire bonds are required on the surface shown.

The Maverick system was designed for a compact missile seeker and uses a comparatively smaller array of 16 elements. These elements are arranged in four groups of four to provide four parallel scan lines, each with four detectors in a time-delay-integration circuit to increase the signal-to-noise ratio. Figure 14 shows a group of Maverick arrays on HgCdTe wafer.

LWIR HgCdTe photoconductors have also been widely used in NASA and NOAA applications for a variety of earth satellite missions. Atmospheric sounders based on the absorption edge of the 14 μm CO_2 band have employed PC HgCdTe devices operating at 90K for more than 20 years. Recently, attention has been focused on monitoring long-term changes to the climate and weather. The Moderate Resolution Imaging Spectrometer – MODIS – instrument has been built to cover 36 spectral bands from visible through LWIR. Operating at 90K, the six longest bands are covered using PC HgCdTe. The MODIS LWIR focal plane is shown in Fig. 15.

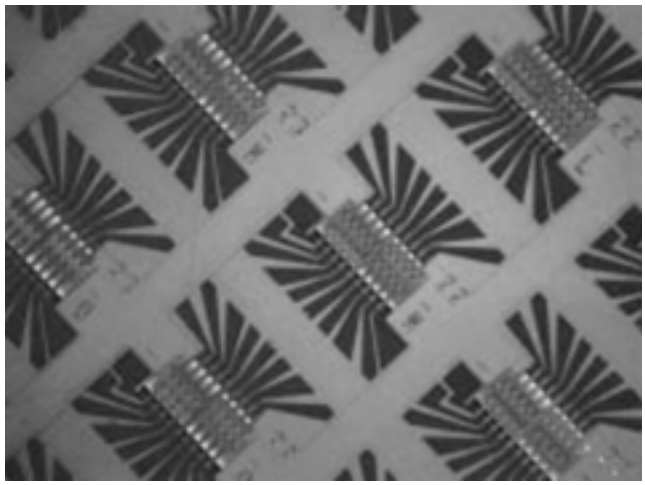

Fig. 14. Maverick arrays on a HgCdTe wafer. These arrays have 16 elements arranged in four groups of four.

A novel variation of the standard photoconductor – the SPRITE detector – was invented in England [19] and a family of thermal imaging systems now utilize this device. The SPRITE detector provides signal averaging of a scanned image spot. This is accomplished by synchronization between the drift velocity of minority carriers along the length of photoconductive bar of material and the scan velocity of the imaging system. The drift velocity is tuned by varying the detector bias. With the two velocities syn-

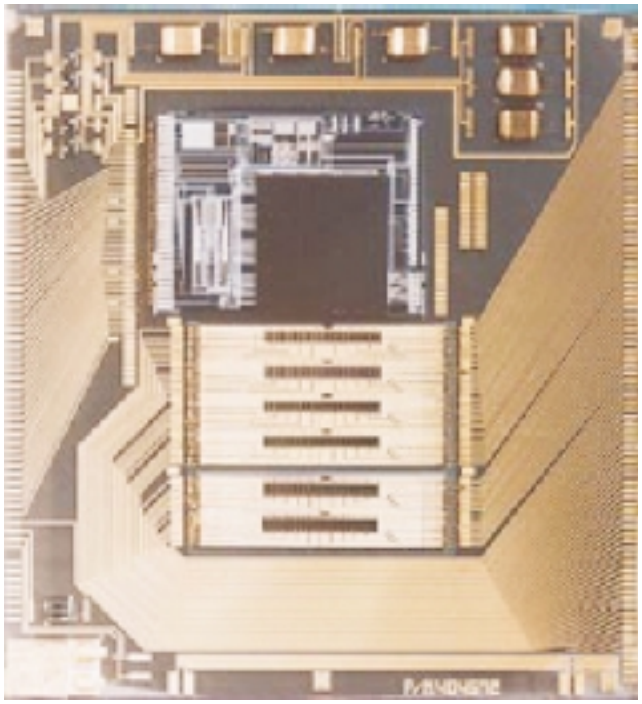

Fig. 15. PC HgCdTe arrays configured in this focal plane are used for six MODIS LWIR spectral bands.

chronized, the image signal builds up a bundle of minority charge which is collected at the end of the photoconductive bar, effectively integrating the signal for a significant length of time and thereby improving the signal-to-noise ratio. The SPRITE device structure is illustrated in Fig. 16.

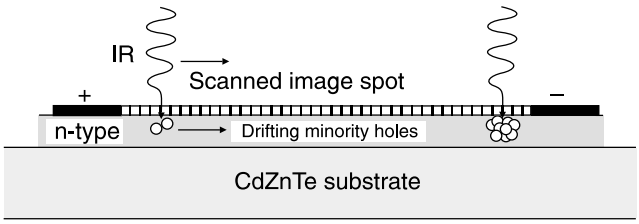

Fig. 16. Cross section of a SPRITE photoconductive detector. The drift velocity of minority carriers is synchronized with the velocity of the scanned image. This integrates the photosignal for an extended length of time and improves the signal-to-noise ratio.

Although first-generation devices are now being widely supplanted by second-generation photovoltaic detectors, the production of these devices will continue for many years to come in support of the large number of systems now in the field.

4.3. Photodiodes

Second-generation HgCdTe devices are two-dimensional arrays of photodiodes. Photodiodes having modest impedance (resistance-area product or R_0A) of 10 $\Omega\,cm^2$ can be mated to silicon readout arrays with indium bump bonds at the pixel level. First demonstrated in the mid-70s [20], indium bump bonding of readout electronics provides for multiplexing the signals from thousands of pixels onto a few output lines, greatly simplifying the interface between the vacuum-enclosed cryogenic sensor and the system electronics. In a general sense, the signal-to-noise ratio of a sensor will improve with the square root of the number of detector elements in an array – to the extent that they can collect proportionally more signal from the scene. Today, millions of pixels are connected to millions of amplifiers/integrators in the unit cells of readout circuits. Figure 17 shows a region of pixels on a 1024×1024 HgCdTe array with indium bumps deposited for bump bonding to readout.

In spite of the tremendous impetus offered by large PV array development, photovoltaic HgCdTe took many years to emerge from laboratory demonstrations. The structure of a mesa-etched photodiode is illustrated in Fig. 18.

The key technology needed to make photovoltaic devices possible was surface passivation. Based on silicon's success, passivation efforts were initially focused mainly on oxides. Anodic oxide was adequate for photoconductors, but the resulting surfaces were heavily accumulated with fixed positive charge. Although the surface shunt this produced did reduce the photoconductive signal, the positive charge minimized surface recombination of minority carriers and that was beneficial. Applied to photodiodes on the other hand, anodic oxide shorted out the devices by inverting the p-type surface.

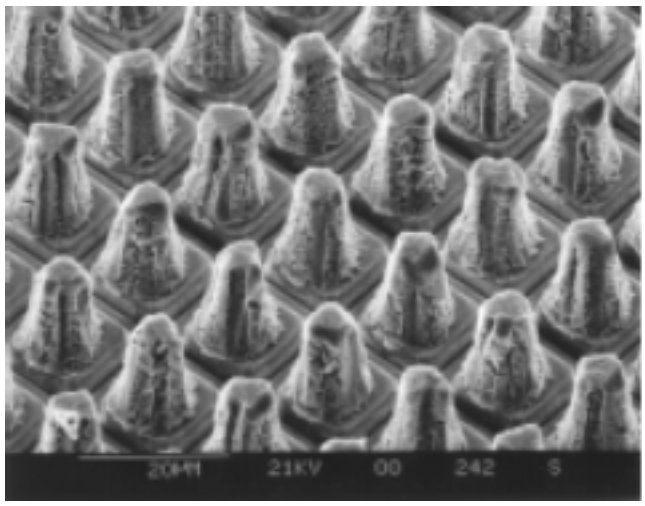

Fig. 17. HgCdTe photovoltaic array with indium bumps. This scanning-electron microscope image shows a portion of an array of 1024×1024 pixels on 17 µm centres.

Silicon oxide was employed for passivation of HgCdTe in the early 80s based upon low-temperature deposition using a photochemical reaction. SiO_2 could be deposited with low surface state densities and excellent PV device properties were demonstrated with this passivation material. However, the excellent surface properties could not be maintained when the devices were heated in vacuum for extended periods of time, a procedure required for good vacuum packaging integrity. These oxides were also subject to surface charge buildup when operated in a space-radiation environment.

ZnS, a common antireflection coating for PC HgCdTe, was used with intermittent success but also lacked stability during vacuum baking. Many other materials were also

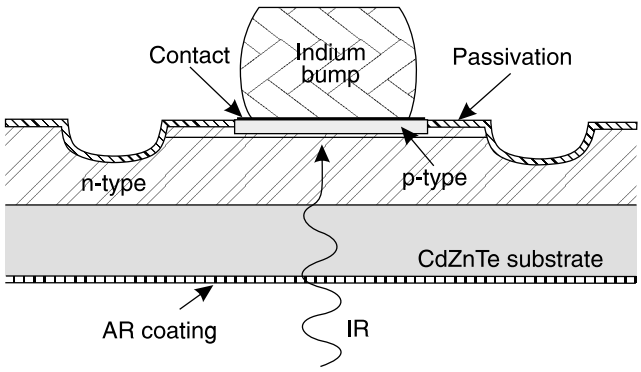

Fig. 18. Cross section of a mesa-etched HgCdTe photodiode. An n-type layer of HgCdTe is grown on a CdZnTe substrate, followed by a p^+-layer to form the junction. Mesa etching defines the individual diodes. The surface is passivated to prevent surface accumulation or inversion. Contacts are made to the p^+-layer in each pixel and to the n-type layer at the edge of the array (not shown). Infrared flux is incident through the IR-transparent substrate.

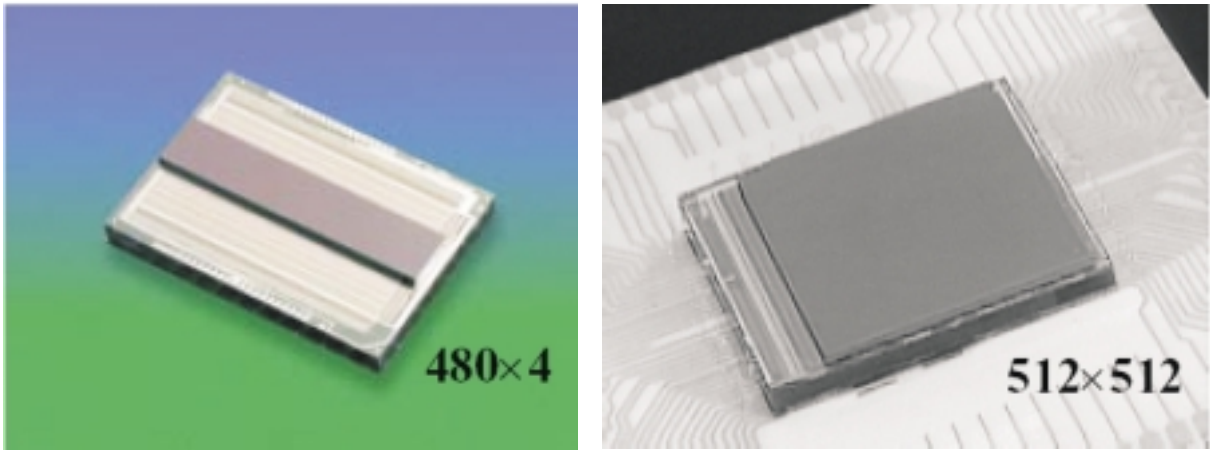

Fig. 19. Examples of second-generation PV HgCdTe detectors which are configured in both scanning (a) and staring (b) formats.

tried with varying success, including oxides, sulfides, and fluorides.

With the advent of CdTe passivation in 1987, HgCdTe photodiodes could finally be reliably passivated. CdTe passivation is stable during vacuum packaging bake cycles and shows little effect from the radiation found in space applications. Diodes passivated with CdTe have been demonstrated which do not show a variation in R_0A with diode size, indicating that surface perimeter effects can be inconsequential. This development has made possible the full-scale production of second-generation devices.

Second-generation HgCdTe photodiodes are now being demonstrated and produced in both scanning and staring formats. Figure 19 illustrates an example of both configurations. For scanned infrared imaging systems the two-dimensional format allows signal averaging through time-delay-and-integration (TDI) signal processing, either on or off the focal plane. Scanning second-generation sensors improve both sensitivity and spatial resolution through the use of more detector elements in both scan and cross-scan directions. Scanning array configurations have increased pixel counts by a significant factor over first-generation arrays – with arrays of 240×4, 288×4, and 480×4 replacing 60, 120, or 180 element arrays.

Staring array configurations have increased the number of pixels even more dramatically over first-generation infrared systems. This has the largest impact on short- and medium-wavelength applications where most or all of the frame time can be used for signal integration. In the long wavelength spectral region, the photon flux from earth scenes will typically fill the unit cell charge storage capacitor in just a fraction of the frame time, limiting the full signal averaging advantage of staring technology. Even so, the improvement over LWIR scanned sensors is significant. Starring array size progression is summarized in Fig. 20 which compares the growth of pixel count over time for a variety of detector technologies with the exponential increase in production DRAM computer memory bits per chip.

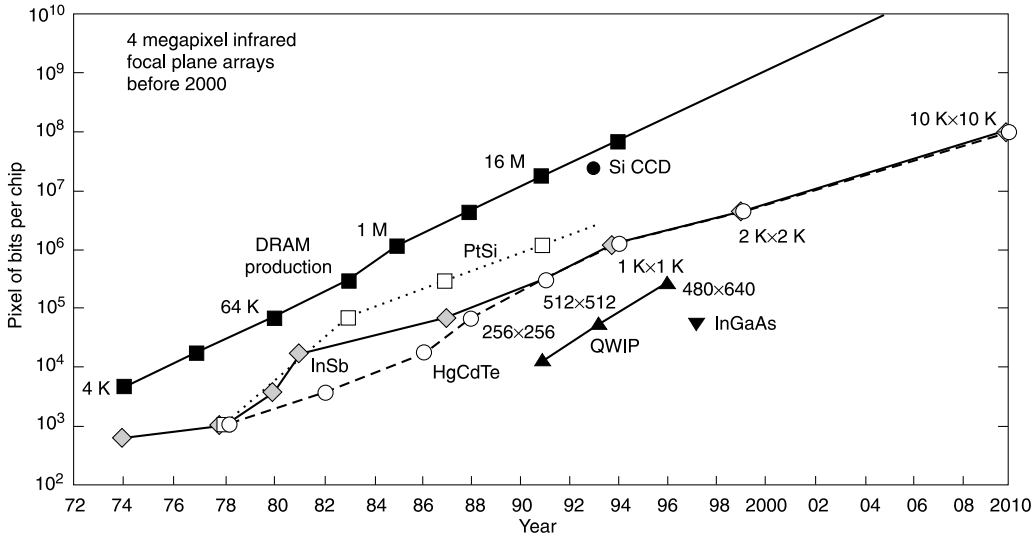

Fig. 20. Progress in infrared staring focal plane array pixel count for a variety of detector materials, including HgCdTe, compared with the exponential increase in DRAM bits per chip since 1972.

Both computer memory chips and infrared focal planes rely on the progression of silicon integrated circuit processing technology because silicon readouts have paced the development of large focal planes. Focal plane pixel count remains below the DRAM growth curve for a two main reasons. First, DRAM technology requires only one transistor per bit, while focal plane readouts require a minimum of three. Second, the market for focal planes is a tiny fraction of that for computer memory and the foundries available for readout fabrication are typically one or two upgrades behind those used for state-of-the-art memory chip builders.

Large staring focal plane evolution has been driven by astronomy applications. This is somewhat surprising given the comparative budgets of the defence market and the astronomical community. The reason astronomers fund large focal plane development is the payback they get in telescope throughput. Large arrays dramatically multiply the data output of a telescope system – in the past decade focal planes designed for astronomy have gone from 64×64 to 2052×2052 an increase of over 1000! Figure 21 shows examples of several large readout wafers from the largest astronomy-array configurations.

The quality of HgCdTe photodiodes – measured by the R_0A product or by leakage current – has improved steadily over the past twenty years as materials and device processing science evolved. There is a recognition that longer wavelength devices are typically more difficult to produce than medium or short wavelength diodes. A decade ago the technology was established to begin production of tactical long wavelength (10 μm) arrays with R_0A products on the order of 10-to-l00 Ω cm^2. Today such devices are routinely produced with very high yield. Diode performance representative of average array quality for a spectrum of HgCdTe alloys is illustrated in Fig. 22.

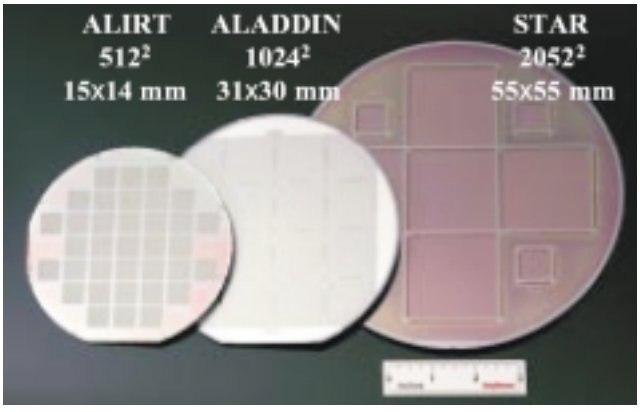

Fig. 21. Readouts for large astronomy array, utilize ever increasing wafer dimensions of 4, 5, and 8 inches (100, 125, and 200 mm). Unlike DRAM, the unit cell size of readouts does not shrink substantially with each design iteration because the pixel size is constrained by the wavelength of infrared radiation and the limits of optical focusing. These readouts are used with both InSb and HgCdTe detector arrays.

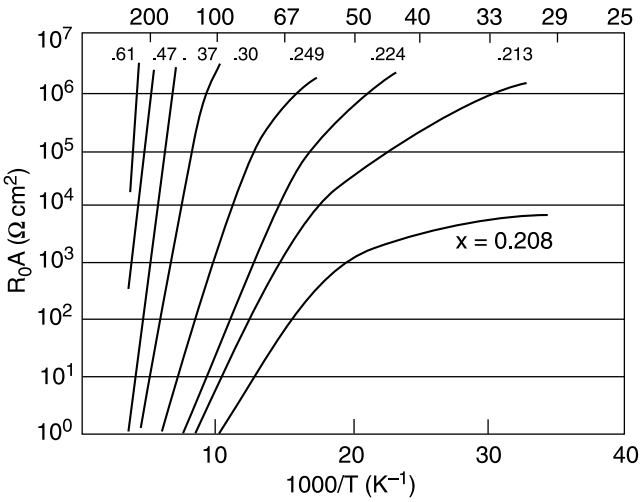

Fig. 22. Performance of a variety $Hg_{1-x}Cd_xTe$ photodiodes made from a range of alloy compositions, as illustrated by the R_0A of the average array diode as a function of inverse temperature.

To appreciate the accomplishments reflected in Fig. 22, one needs to know the relationship between detectivity, D^* and R_0A. D^* is a figure-of-merit for infrared detectors which is independent of system parameters such as the optical configuration, and independent of detector element size [21]. Ideal detectors are limited by statistical fluctuations of the background radiation incident on the detector – assuming the detector noise itself is insignificant compared with the quantum fluctuations in the arrival of photons. State-of-the-art HgCdTe and InSb infrared detectors approach this limit within a factor of two or better over a wide range of photon-flux conditions. For the detector noise to be insignificant, the detector leakage current must be low, or conversely the detector impedance must be high. The detector impedance required to achieve a certain D* is given by the expression:

$$D^* = \frac{\eta q \sqrt{R_0 A}}{2E_\lambda \sqrt{kT}}, \qquad (2)$$

where η is the quantum efficiency, q is the electronic charge, E_λ is the energy of the photon, and k is Boltzmann's constant. This relationship is plotted for short, medium, and long wavelength examples in Fig. 23 for a representative temperature of 80 K. Note that D^* varies with the square root of R_0A and the inverse square root of temperature.

Second-generation PV HgCdTe technology is now capable of being produced for a variety of low-background strategic applications as well higher-background flux tactical applications. Work is still underway to push the performance of long wavelength detectors – 14 μm and greater – to higher levels for critical applications such as monitoring the earth's atmosphere from spacecraft. In parallel with these efforts, a third generation of HgCdTe devices has emerged as described in the following section.

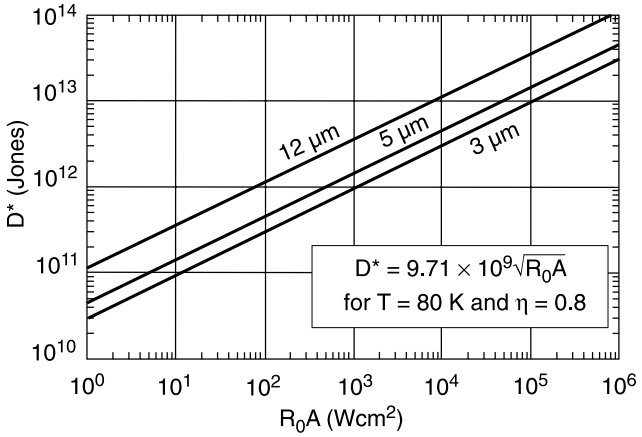

Fig. 23. D* as limited by R_0A product, illustrated for photon energies representative of short, medium, and long wavelengths, and at a temperature of 80 K. D* may be limited by other mechanisms than R_0A in practice, such as statistical fluctuations in the arrival of background photons.

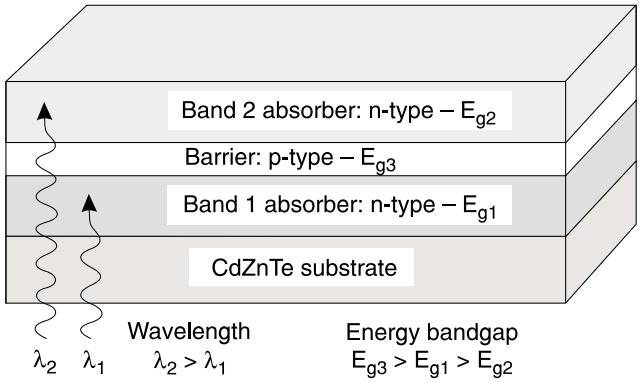

Fig. 24. Structure of a HgCdTe two-colour detector pixel. Infrared flux from the first spectral hand is absorbed in the Band 1 epitaxial layer, while longer wavelength flux is transmitted through the Band 1 layer and absorbed in the Band 2 layer. A thin p-type barrier layer separates the two absorbing bands.

5. Third generation HgCdTe devices

The definition of third-generation devices is not particularly well established. Here it is taken to mean device structures that have substantially enhanced capabilities over an ordinary photodiode. We will describe three such examples:

- Two colour detectors.
- Avalanche photodiodes.
- Hyperspectral arrays.

The technical developments which are key to third-generation devices include dry etching, vapour-phase epitaxy, optical coatings, and advanced readout concepts.

5.1. Two colour detectors

The virtues of colour vision are easily appreciated in the visible because colour is a powerful discriminator of everyday objects. For infrared systems, sensitivity in dual spectral bands has been demonstrated to have similar virtues [22].

Dual band sensors have been demonstrated using two focal planes and a beam splitter. This works, but there is considerable difficulty in optical alignment to a precision such that the exact same image feature can be accurately compared on the two focal planes at the pixel level. It also has the drawbacks of dual vacuum enclosures and cooling systems.

Two colour detectors are a remarkable solution to the problem of pixel registration in dual band sensors [23]. Two-colour detectors are made with a stack of two detector layers separated by a common electrode, in the case of HgCdTe, a p-type layer. Figure 24 illustrates the structure. The Band 1 and Band 2 alloy compositions can be any two x-values as long as Band 1 has a higher x-value than Band 2. Although this structure can be grown by LPE methods, vapour phase growth is the preferred method.

At this time two colour detectors have been successfully demonstrated in a variety of spectral combinations. Figure 25 shows three such examples.

There are two variations of the two-colour detector structure. The first type, the sequential two-colour detector, has just one indium bump per pixel. Each band is read in turn by reverse biasing the diode from which the signal is desired. The device structure appears as a floating-base *npn* transistor, and care must be taken to avoid bipolar gain due to injection into the base.

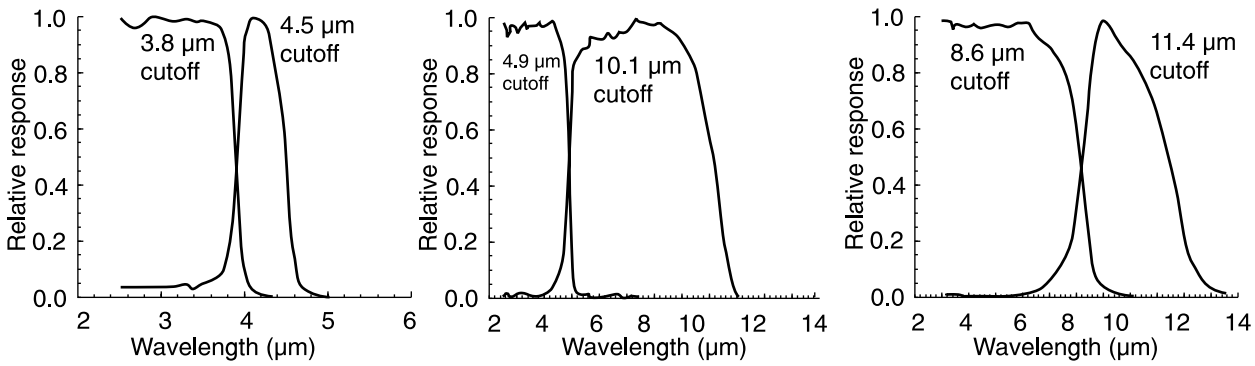

Fig. 25. Examples of HgCdTe two-colour detectors. Note that the high absorption coefficient of HgCdTe in Band 1 limits the spectral crosstalk from Band 2 to low values.

The second type of two-colour detector has two indium bumps per pixel and is called a simultaneous two-colour detector. Signals are read from the Band 2 layer and from the p-type barrier layer, allowing extraction of the signals from both bands simultaneously. The meaning of "simultaneously" must be defined by the system user, since it is frequently the case that the length of signal integration may be different for each band. Figure 26 shows the structure of a simultaneous two-colour pixel.

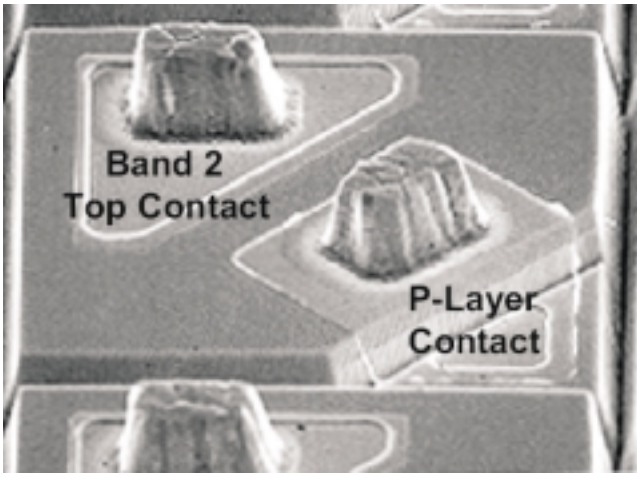

Fig. 26. Structure of a simultaneous two-colour pixel. One indium bump contacts the n-type layer of Band 2. The other bump contacts the p-type layer between Band 1 and Band 2.

In addition to the importance of vapour phase epitaxy in growing the three-layer HgCdTe structure for two-colour detectors, the development of anisotropic dry etching was important in being able to make these devices in smaller pixel sizes. This is because the mesa etch of a two-colour detector is relatively deep – on the order of 12 μm – as may be seen in Fig. 26. Without anisotropic etching, much of the mesa would be consumed in isolating adjacent pixels.

Two-colour detectors in both sequential and simultaneous modes have been demonstrated in imaging systems. Figure 27 illustrates a two colour infrared image in which a circular filter is opaque in one band (on the left) and transparent in the other band (on the right). The wide variety of applications made possible by these devices is anticipated to inspire the development of many future systems based on this technology.

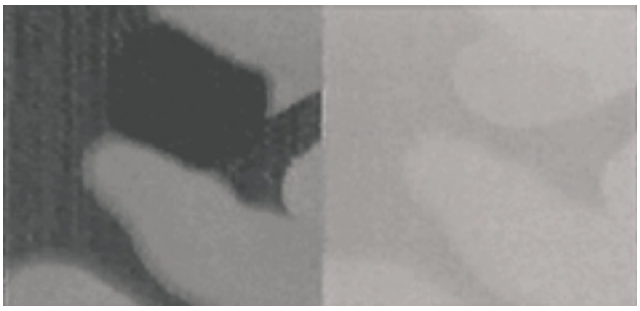

Fig. 27. Two-colour infrared camera image. A circular filter being held in the hand is opaque in Band 1 shown on the left, and transparent in Band 2 on the right allowing the finger tip to be seen through the filter.

5.2. Avalanche photodiodes

Short-wavelength HgCdTe avalanche photodiodes (APDs) are able to exploit a very favourable property in the band structure of the alloy when the bandgap is about 0.90 eV. For materials of this alloy composition, the energy required to excite an electron from the top of the valence band to the bottom of the conduction band is identical to the energy for the excitation of an electron from the top of the split-off valence band to the top of the valence band. For the right-brained reader, the somewhat complicated description just stated is illustrated in Fig. 28.

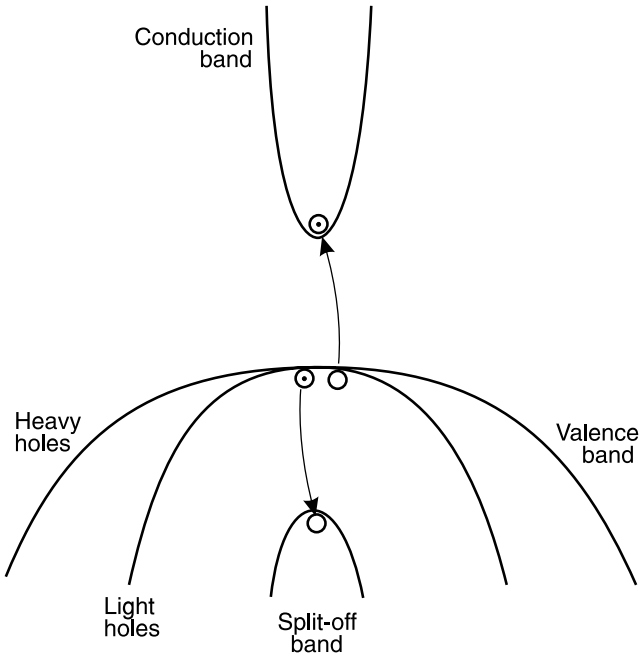

Fig. 28. Band structure of HgCdTe for alloy compositions at which the bandgap is about 0.90 eV, corresponding to 1.37 μm. At this composition, the split-off band is separated from the top of the conduction band by the same energy. This resonance condition allows very favourable multiplication of holes.

The avalanche effect in the high-field region of an avalanche photodiode multiplies the number of photoexcited carriers by the avalanche gain. This raises the signal level, which itself may be highly useful for raising low signal levels above the amplifier noise. A second consideration is the amount by which the noise is increased by the avalanche process. Here it is advantageous to have a large asymmetry between the avalanche gain of holes and electrons. The band structure of HgCdTe gives k-values of 0.1 or less – a highly favourable ratio of hole to electron multiplication during avalanche conditions, resulting in very little noise gain.

These properties give HgCdTe APDs a figure of merit four times better than InGaAs APDs. Applied to systems, the result is detection range twice that for competing III-V devices, giving them significant leverage for many applications.

A number of avalanche structures have been built and demonstrated in HgCdTe for detection at 1.06, 1.3, and 1.55 μm. Initial demonstrations utilized LPE grown structures, but MBE growth is now chiefly used. Figure 29 illustrates one such APD structure which consists of six MBE-grown layers [24]. Complex HgCdTe device structures such as those grown for two-colour arrays and APDs are a testimony to the recent maturation of vapour phase growth technology.

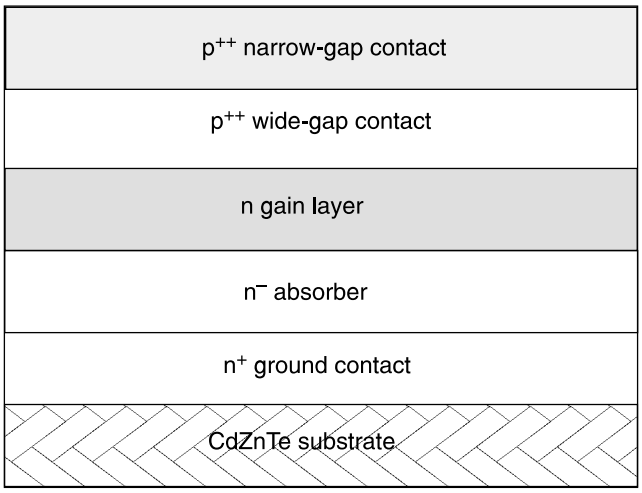

Fig. 29. Avalanche photodiode structure consisting of six HgCdTe layers. The alloy composition of the avalanche gain layer is tuned to the energy resonance condition illustrated in Fig. 28. Layers adjacent to the absorber layer typically block wavelengths shorter than the absorption-layer peak response, giving a spectrally-narrow response as shown in Fig. 10.

A photo of a 5×5 array of 50 μm APDs is shown in Fig. 30. HgCdTe APDs are especially attractive for array applications. This is because the material properties favour uniform avalanche gain across an array compared to the properties of competing devices. More specifically, the fractional variation in gain as a function of electric field is lower in HgCdTe than in silicon or InGaAs. Array applications are also attractive because the device yield is comparatively high in HgCdTe material. An example of this for a 5×5 array is illustrated in Fig. 31, showing a tight distribution of voltages at which a gain of 10 is achieved and high yield of working diodes.

APDs must have low dark currents, since the dark current will be multiplied in the device along with any photocurrent. Figure 32 shows the dark current, the gain, and the normalized dark current as a function of bias for HgCdTe APD with a 1.65 μm cutoff measured at 295 K. Gain as high as 100 was measured in this device. Note that the dark current normalized to the gain decreases above

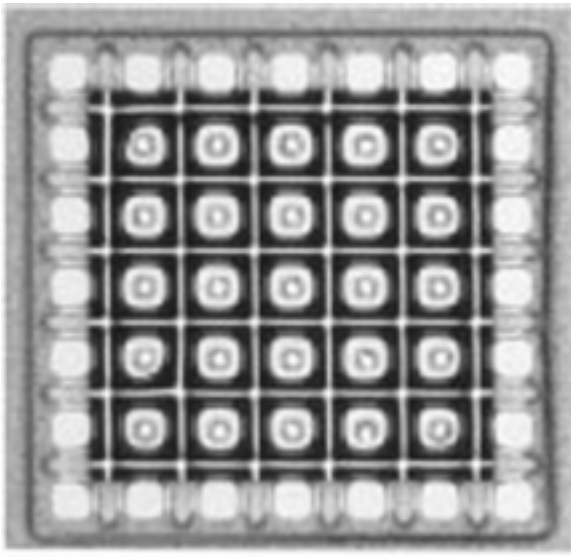

Fig. 30. 25-element HgCdTe array of avalanche photodiodes.

75 V. This is indicates that the dark current at low gain is dominated by surface leakage which is not subject to the avalanche effect.

HgCdTe APDs are attractive for specialized applications where maximum detector performance leverages the utility of system. Table 2 summarizes the properties and performance for a variety of APD sizes from 50 to 300 μm diameter measured at 1.55 μm. Single elements together with both linear and two-dimensional arrays of these devices are currently being demonstrated in advanced applications. With a bandwidth exceeding 1 GHz and with near-ideal avalanche properties, these devices will find a variety of applications in future systems in which detector performance has high leverage on the system cost and capability.

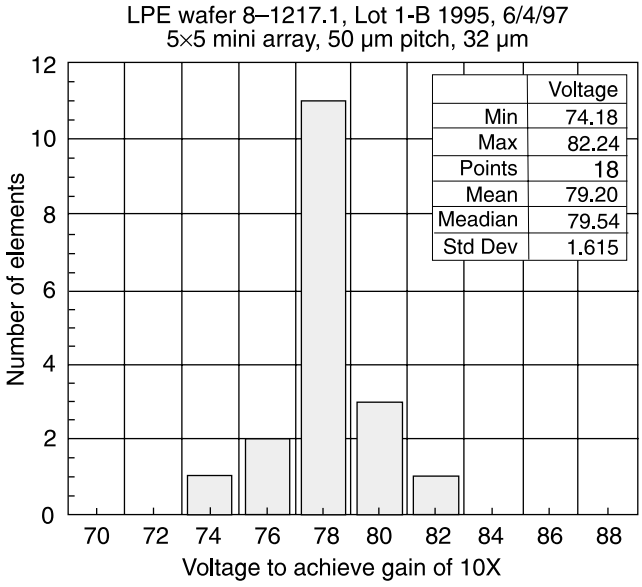

Fig. 31. Good uniformity of bias voltage to achieve a gain of 10 for a 5×5 array of 1.65 μm cutoff HgCdTe APDs.

Table 2. Properties and performance of a variety of HgCdTe APDs ranging in size from 50 to 300 μm diameter.

Diameter (μm)	Bias (V)	Responsivity (A/W)	η×G	Noise (pA/√Hz)	Total I_{dark} (nA)	NEP (nW)	Capacitance (pF)
50	77.7	13.1	10.6	1.9	66	0.92	0.2
100	72.9	12.4	9.9	1.4	120	0.72	0.3
200	76.9	12.8	10.2	3.6	580	1.8	0.8
300	68.9	12.5	10	3	810	1.6	1.6

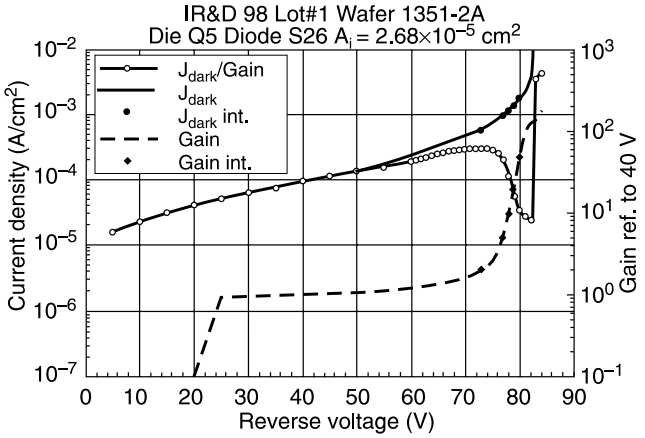

Fig. 32. Gain (right scale), dark current density (J_{dark}), and dark current density normalized to gain ($J_{dark}/Gain$) for a 1.65 μm cutoff HgCdTe APD. Gain up to 100 is achieved in this device together with low normalized dark current density.

5.3. Hyperspectral arrays

When a second-generation array is combined in a scanning imager having a means to selectively illuminate each row with a different spectral band we have a hyperspectral imager. Such instruments can image a scene in hundreds of spectral bands per frame, generating a hypercube image. Such a capability is anticipated to revolutionize disciplines such as land resource utilization which today rely on just a handful of spectral bands.

In a hyperspectral application, standard second-generation HgCdTe arrays are enhanced with more elaborate optical coatings and/or proximal filters. One example is the wedge-filter spectrometer hyperspectral array. In this case a narrow-band spike filter is deposited with the thickness of each coating layer uniformly graded across one dimension of the filter substrate. The gradation is designed to achieve a specific variation in wavelength across the detector rows. Figure 33 illustrates the assembly configuration. When used with a grating or prism as the spectral-dispersing element, the wedge filter is replaced with a wedged antireflection coating.

Hyperspectral arrays have been built to cover the visible through LWIR spectral regions [25]. HgCdTe and other detector materials such as silicon and InSb have been used in hyperspectral assemblies.

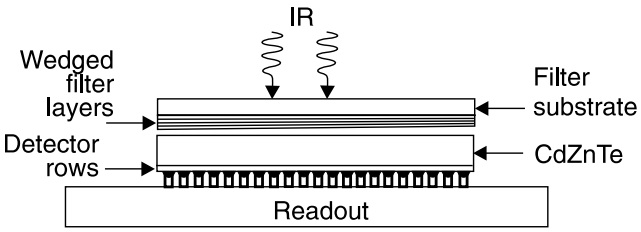

Fig. 33. Cross section of a wedge-filter hyperspectral HgCdTe array.

6. Summary and conclusions

HgCdTe has emerged as the most widely used infrared detector today because of its excellent properties, including:

- The alloy composition can be optimised for any wavelength in the range of 0.7–20 μm.
- Quantum efficiency is very high.
- Minimal cooling is required because the detection mechanism relies photoexcitation across an intrinsic bandgap.
- The R_0A product (or inversely the leakage current) responds to cooling.
- D^* varies with the background flux, improving as the flux is lowered from high to low background levels.
- Growth technology has matured.
- Compositional uniformity is excellent, even in the VLWIR region [26].
- Sophisticated device structures can be grown by vapour phase for third-generation applications.

In the future, HgCdTe technology will continue to expand the envelope of its capabilities. Progress is anticipated in the development of:

- Larger arrays – this will be possible with the growth of HgCdTe directly on silicon substrates.
- Longer wavelength response – current efforts should firmly establish the capability to produce second-generation arrays in the very LWIR range of 14–20 μm for demanding space applications.
- Reduced cooling requirements with no loss of performance for HgCdTe detectors are anticipated with improving material properties and innovative device designs.
- Faster readouts will improve the effective duty-cycle (ratio of integration time to frame time) of LWIR arrays

at high background levels, improving the sensitivity for many applications.
- Three colour arrays will provide additional flexibility to the system user.

Acknowledgments

Colleagues in Santa Barbara and elsewhere in the industry have established the breadth of capabilities summarized in this paper. Tse Tung has graciously helped review the materials on comparative growth techniques. Thanks are due to James Bangs, Jeffery Johnson, Libby Patten, and Jerry Wilson for material on two-colour arrays. Michael Jack supplied helpful information on the status of avalanche photodiodes. Geoffery Walter has tutored the author on aspects of wedge filters.

References

1. W. D. Lawson, S. Nielson, E. H. Putley, and A. S. Young, "Preparation and properties of HgTe and mixed crystals of HgTe-CdTe," *J. Phys. Chem. Solids* **9**, 325–329 (1959).
2. D. Long and J. L. Schmit, "Mercury-cadmium telluride and closely related alloys," in *Semiconductors and Semimetals*, Vol. 5, pp. 175–255, edited by R. K. Willardson and A. C. Beer, Academic Press, New York (1970).
3. G.L. Hansen, J.L. Schmit, and T.N. Casselman, "Energy gap versus alloy composition and temperature in $Hg_{1-x}Cd_xTe$," *J. Appl. Phys.* **53**, 7099–7101 (1982).
4. M.W. Scott, "Energy gap in $Hg_{1-x}Cd_xTe$ by optical absorption", *J. Appl. Phys.* **40**, 4077–4081 (1969).
5. Y. Kanai and K. Shohno, "Dielectric constant of PbTe", *Jap. J. Appl. Phys.* **1**, 239 (1962).
6. P.B. Alien and M.L. Cohen, "Carrier concentration dependent superconductivity in tin telluride and germanium telluride", *Phys. Rev.* **177**, 704–706 (1969).
7. L.R.S. Ladd, "Cadmium telluride infrared transmitting material", *Infrared Phys.* **6**, 145–51 (966)
8. V. Prakash, "The optical absorption edge in the lead salts and its variation with temperature and pressure", Harvard University contract NONR-1866 10 NR-017-308, p. 241, AD 656 591, 1967; B. Houston, *et al.* "Elastic constants, thermal expansion, and Debye temperature of lead telluride", *J. Appl. Phys.* **39**, 3913–3916 (1968).
9. H. Ibach, "Thermal expansion of silicon and zinc oxide", *Physics Status Solidi* **31**, 625–634 (1969). Results from a half-dozen earlier papers are summarized in *Integrated Silicon Device Technology*, Vol. V, pp. 20–21, Physical/electrical properties of silicon. Research Triangle Institute, AD 605 558, 7/64.
10. The data in this figure was compiled from a variety of sources. A recent reference which can be consulted is: *Semiconductor Alloys, Physics and Materials Engineering*, by An-Ban Chen and Arden Sher, Microdevices, Physics and Fabrication Technologies, Plenum Press, New York, 1995.
11. M.A. Kinch and A. Yariv, "Performance limitations of GaAs/AlGaAs infrared superlattices," *Appl. Phys. Lett.* **55**, 2093–2095 (1989).
12. B.F. Levine, "Quantum-well infrared photodetectors," *J. Appl. Phys.* **74**, R1–R81 (1993).
13. A. Rogalski and K. Jóźwikowski, "GaAs/AlGaAs quantum well infrared photoconductors versus HgCdTe photodiodes for long-wavelength infrared applications", *Opt. Eng.* **35**, 1477–1484 (1994).
14. A Rogalski and M. Razeghi "Narrow-gap semiconductor photodiodes", *Proc. SPIE* **3287**, 2–13 (1997).
15. A. Singh and D.A. Cardimona, "Design issues related to low dark current in QWIPs", *Proc. SPIE* **2999**, 46–54 (1997).
16. S. D. Gunapala, J. K. Liu, J. S. Park, M. Sundaram, C. A. Shott, T. Hoelter, T. L. Lin, S. T. Massie, P. D. Maker, R. E. Muller, and G. Sarusi, "9-μm cutoff 256×256 GaAs/$Al_xGa_{1-x}As$ quantum well infrared photodetector hand--held camera", *IEEE Trans. Electron Devices* **44**, 51–57 (1997).
17. *Properties of Narrow Gap Cd-based Compounds*, edited by P. Capper, EMIS Datareviews Series, No 10, INSPEC, The Institution of Electrical Engineers, London, 1994.
18. Prior to about 1993 this series was known as *The U.S. Workshop on the Physics and Chemistry of Mercury Cadmium Telluride* and was published by the American Vacuum Society.
19. C.T. Elliott, D. Day, and B.J. Wilson, "An integrating detector for serial scan thermal imaging", *Infrared Phys.* **22**, 31–42 (1982).
20. R. Thorn, "High density infrared detector arrays", U.S. Patent No 4,039,833, 8/2/77.
21. R.C. Jones, "A method of describing the detectivity of photoconductive cells", *Rev. Sci. Instr.* **24**, 1035–1040 (1953).
22. D. Scribner, J. Schuler, P. Warren, M. Satyshur, and M. Kruer, "Infrared color vision: separating objects from backgrounds", *Proc. SPIE* **3379**, 2–13 (1998).
23. E. Schulte, "Two terminal multi-band infrared radiation detector", U.S. Patent No 5,113,076, 5/12/92,
24. T.J. de Lyon, B. Baumgratz, G.R. Chapman, E. Gordon, M.D. Gorwitz, A.T. Hunter, M.D. Jack, J.E. Jensen, W. Johnson, K. Kosai, W. Larsen, G.L. Olson, M. Sen, and B. Walker,"Epitaxial growth of HgCdTe 1.55 μm avalanche photodiodes by MBE", *Proc. SPIE* **3629**, 256–267 (1999).
25. P. Norton, "Status of infrared detectors", *Proc. SPIE* **3379**, 102–114 (1998).
26. M. Weiler, S. Tobin, M. Hutchins, and P. Norton, "Recent advances in composition control for VLWIR HgCdTe heterojunction photodiodes for remote sensing applications at 60 K", *Proc. ECS*, Boston, 1998.

